

# Two types of criticality in the brain

David Dahmen,<sup>1</sup> Sonja Grün,<sup>1,2</sup> Markus Diesmann,<sup>1,3,4</sup> and Moritz Helias<sup>1,4</sup>

<sup>1</sup>*Institute of Neuroscience and Medicine (INM-6) and Institute for Advanced Simulation (IAS-6) and JARA Institute Brain Structure-Function Relationships (INM-10), Jülich Research Centre, Jülich, Germany*

<sup>2</sup>*Theoretical Systems Neurobiology, RWTH Aachen University, Aachen, Germany*

<sup>3</sup>*Department of Psychiatry, Psychotherapy and Psychosomatics, Medical Faculty, RWTH Aachen University, Aachen, Germany*

<sup>4</sup>*Department of Physics, Faculty 1, RWTH Aachen University, Aachen, Germany*

(Dated: March 20, 2018)

Neural networks with equal excitatory and inhibitory feedback show high computational performance. They operate close to a critical point characterized by the joint activation of large populations of neurons. Yet, in macaque motor cortex we observe very different dynamics with weak fluctuations on the population level. This suggests that motor cortex operates in a sub-optimal regime. Here we show the opposite: the large dispersion of correlations across neurons is a signature of a rich dynamical repertoire, hidden from macroscopic brain signals, but essential for high performance in such concepts as reservoir computing. Our findings suggest a refinement of the view on criticality in neural systems: network topology and heterogeneity endow the brain with two complementary substrates for critical dynamics of largely different complexities.

The brain is a dynamical system with potentially different regimes of operation. Network models and experiments suggest optimal computational performance at critical points, which mark the transition between two dynamical regimes [1]. At critical points, systems exhibit universal behavior, characterized by strong concerted fluctuations between all constituents leading to effective long-range interactions despite short-range couplings.

A particular type of criticality occurs in neuronal networks with equal excitatory and inhibitory feedback, leading to neuronal avalanches [2] which are visible as large transients of population activity with a slowly decaying autocorrelation. Signatures of avalanches have also been observed in mesoscopic measures of neuronal activity in macaque motor cortex [3]. However, our parallel neuronal spiking activity in this cortical region does not show such large transients of population activity (Fig. 1B,E) and long-range temporal correlations (Fig. 1F). The data rather show weak and fast fluctuations of the population activity, suggesting an excess of inhibitory feedback and dynamically balanced activity [4], predicting low average correlations [5, 6] as observed in Fig. 1D.

Another type of criticality, devoid of avalanches, has been investigated in computational studies [8]: edge-of-chaos criticality. With increasing heterogeneity in network connections, the dynamics change from regular to chaotic. At the transition point, networks possess rich dynamics: a collection of coexisting network modes leads to topologically complex responses [9]. The onset of chaotic dynamics coincides with the breakdown of linear stability of the deterministic dynamics [10]. A direct measurement of the linear stability is, however, hampered by noise and the sparse sampling of the network dynamics.

We therefore choose correlations in the neuronal activity (Fig. 1D) as an indirect measure. They are informative, because they arise from interactions between neurons, which cause the collective behavior. Pairwise covariances, to a good approximation, follow the unique and model-invariant law [11–13]

$$c(W) = [1 - W]^{-1} D [1 - W^T]^{-1}, \quad (1)$$

which relates the pairwise covariances  $c(W)$  to the effective connectivity matrix  $W$  of the linearized dynamics. The latter is the product of the anatomical connectivity and the sensitivity of individual neurons. The matrix  $D$  can be determined from firing rates, shared and correlated external inputs, but the final results turn out to be independent of  $D$ .

The linearized network dynamics corresponding to Eq. (1) become unstable if one eigenvalue of  $W$  has a positive real part ( $\text{Re}(\lambda) \geq 1$ ). Eigenvalues are, in principle, determined by all connections in the network. But their determination from experimentally observed covariances by Eq. (1) is hindered by severe subsampling; even with massively parallel recording techniques, at most hundreds of neurons can be measured simultaneously from the same local network. We therefore need to find a characteristic of the correlations that is informative about the eigenvalues, insensitive to the details of the network, and that can be estimated from a few hundred neurons at most.

We first study theoretically how the distribution of covariances is affected by the heterogeneity of connections (Fig. 2). In a sparse network with fixed connection probability, the heterogeneity is uniquely given by the strength of connections. With increasing connection strength, activity successively propagates over multiple synapses, leading to

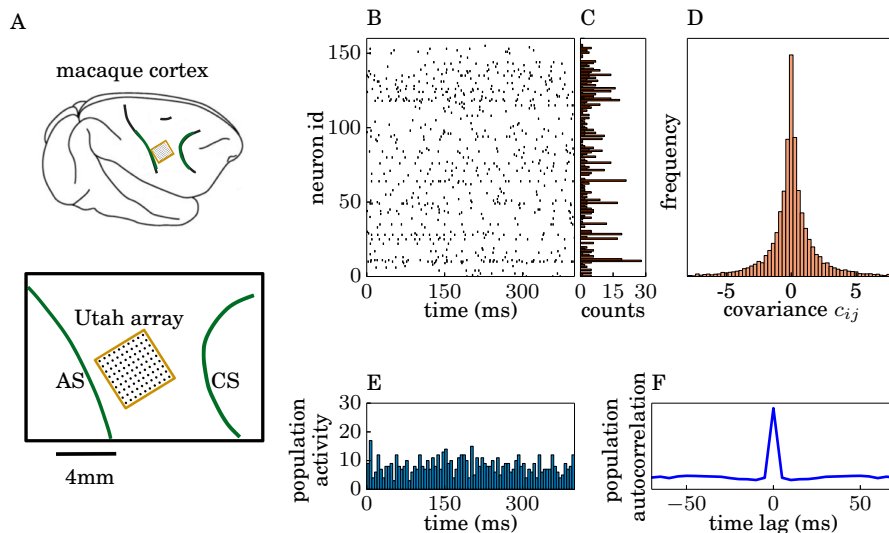


Figure 1. **Spiking activity in macaque motor cortex.** (A)  $10 \times 10$ -electrode “Utah” array (Blackrock Microsystems, Salt Lake City, UT, USA; black dots) with  $400 \mu\text{m}$  interelectrode distance covering an area of  $4 \times 4 \text{ mm}^2$  (yellow square) of macaque motor cortex between the arcuate (AS, left green curve) and the central sulcus (CS, right green curve) of the right hemisphere. (B) Single trial raster plot of spiking activity of 155 neurons within  $T = 400 \text{ ms}$  after trial start (TS) of a reach-to-grasp task [7]. (C) Spike counts  $n_i$  of activity within  $T = 400 \text{ ms}$ . (D) Distribution of covariances  $c_{ij} = \frac{1}{T} (\langle n_i n_j \rangle - \langle n_i \rangle \langle n_j \rangle)$  between spike counts  $n_i$  in 141 trials. (E) Time-resolved population activity binned in  $t_{\text{bin}} = 5 \text{ ms}$ . (F) Autocorrelation function of binned population activity.

indirectly mediated interactions via a growing number of parallel paths (Fig. 2A) [12, 13]. The eigenvalues of the connectivity matrix approach the critical line where the dynamics lose linear stability (Fig. 2B). Distributions of covariances (Eq. 1) become monomodal and broader but stay centered approximately around zero (Fig. 2C,D). These results expose a unique hallmark of dynamically balanced networks that operate close to linear instability: widely distributed covariances with a small mean as we observe in the motor cortex (Fig. 1D).

Although local cortical networks show non-random, cell-type specific, and distance-dependent connectivity, the simple model of a homogeneous random network studied in Fig. 2 is sufficient to explain gross features of the experimental data. To calculate the dispersion of covariances, we apply a well-established analytical technique for disordered physical systems: instead of considering all pairwise covariances in a single network, we observe the covariance of an individual pair of neurons in different network realizations. The connectivity appears as an inverse matrix in Eq. (1), which technically complicates the analysis: no results from random matrix theory apply to this particular problem. Instead we construct a moment generating function [14] for the linearized network dynamics [18], which allows for the use of spin-glass techniques [15, 16] combined with approximations for large- $N$  field theories [17]. As a result, the disorder contained in the  $\sim N^2$  entries of the connectivity formally reduces to only two fluctuating auxiliary variables that provide input to a fully symmetric all-to-all connected network. Only this high symmetry and the drastic reduction of dimensionality enables us to obtain a mean-field theory that describes the neuron-to-neuron variability [18]. This theory yields the mean and standard deviation of variances ( $i = j$ ) and covariances ( $i \neq j$ ) to leading-order in the network size  $N$ :

$$c_{ij} = \left[ [1 - \mu]^{-1} D_\lambda [1 - \mu^T]^{-1} \right]_{ij}, \quad (2)$$

$$\delta c_{ij} = \sqrt{\frac{1 + \delta_{ij}}{N} \left( \left( \frac{1}{1 - \lambda_{\text{max}}^2} \right)^2 - 1 \right) D_\lambda}. \quad (3)$$

Here,  $\mu_{ij} \sim \mathcal{O}(1/\sqrt{N})$  is the mean and  $\sigma_{ij}^2 = \lambda_{\text{max}}^2/N \sim \mathcal{O}(1/N)$  is the variance of connection weights in  $W$ . The latter determines the radius  $\lambda_{\text{max}}$  of the bulk of eigenvalues (Fig. 2B) and the renormalized matrix  $D_\lambda = D/(1 - \lambda_{\text{max}}^2)$ , which accounts for the structural variability of connections. Eq. 2 predicts that the mean covariances are low ( $c_{ij} \sim \mathcal{O}(1/N)$ ) if the network is inhibition dominated ( $\mu < 0$ ) [5, 6]. For large spectral radii  $\lambda_{\text{max}} \lesssim 1$ , Eq. (3), moreover, predicts a large standard deviation ( $\delta c_{ij} \sim \mathcal{O}(1/\sqrt{N})$ ) as experimentally observed in our data (Fig. 1D).

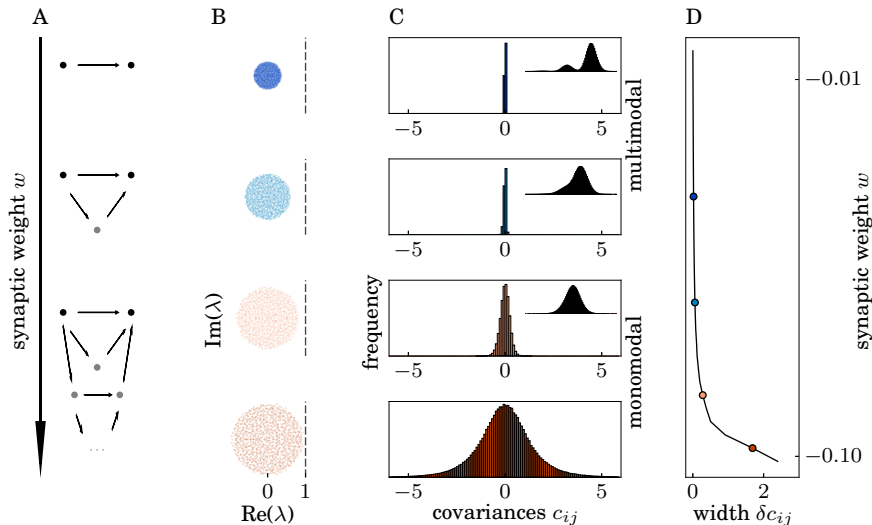


Figure 2. **Dispersion of correlations measures stability of network dynamics.** Connection strength  $w$  in a sparse random network increases from top to bottom (vertical axis). (A) Connections (arrows) between a pair of observed neurons (black dots); indirect connections contribute to correlations via intermediate neurons (gray dots). (B) Bulk eigenvalues  $\lambda$  (colored dots) of the connectivity matrix  $W$  in the complex plane (critical line at  $\text{Re}(\lambda) = 1$ ). (C) Distributions of covariances (Eq. 1). Enlargement shown as insets. (D) Standard deviation  $\delta c_{ij}$  of distribution of covariances (black curve; colored symbols correspond to distributions shown in panel C).

The theory, in principle, determines the largest eigenvalue from measured covariances. But there are two complications:  $D_\lambda$  is not known and cannot be measured, and it is unclear how robust the result is with regard to more realistic connectivity. Both problems are solved by considering the normalized width of the distribution of covariances  $\Delta = \delta c_{ij}/c_{ii}$ . This measure is predominantly determined by the network size and the most unstable eigenvalue,  $\lambda_{\max}$  (Fig. 3C). The prediction of  $\Delta$  is sufficient even for network topologies such as excitatory-inhibitory networks (Fig. 3F) and distance-dependent connection probabilities (Fig. 3G). The latter networks also qualitatively explain the shape of the experimentally observed covariance distribution. The applicability of the theory goes beyond linear network dynamics; it predicts  $\Delta$  even in spiking networks (Fig. 3H). Therefore, the normalized width  $\Delta$  can be used to infer the operational regime of the cortical network (Fig. 1). The distance to linear instability is determined by  $\lambda_{\max}$  which, to leading order in  $N$ , is given by inversion of Eqs. (2) and (3) as

$$\lambda_{\max} = \sqrt{1 - \sqrt{\frac{1}{1 + N\Delta^2}}}. \quad (4)$$

The dispersion measured in massively parallel spike recordings of macaque motor cortex (Fig. 1D) predicts that the network operates close to instability (Fig. 3D). Biologically plausible neuron numbers  $N$  below the recording array are above  $10^4$ . Together with the measured relative width  $\Delta = 0.15$  (with bias correction due to the finite amount of measured data [18]) this leads to a small quantity  $N\Delta^2$ , such that Eq. (4) predicts  $\lambda_{\max} \lesssim 1$  (Fig. 3D, gray area).

In general, a value  $\lambda_{\max} \lesssim 1$  results from the large heterogeneity of connections across neuron pairs. It implies a large number of eigenvalues of the effective connectivity matrix being close to the critical line where linear stability breaks down (Fig. 4A). Due to the proximity of the eigenvalues to this critical line, the network possesses a rich dynamical repertoire of multiple-neuron responses (modes) with different time courses (Fig. 4C). The contribution of each neuron to a particular mode is different for each neuron and determined by the eigenvector of the connectivity matrix corresponding the mode (Fig. 4A, cyan bars). Many modes have large time constants that would be visible in slowly decaying autocorrelation functions (Fig. 4C). However, a direct experimental identification of these modes is a major challenge. The often-considered population activity is only one particular mode where all neurons contribute equally. The almost vanishing mean of the covariances (Fig. 1D, Fig. 4B) and the weakly fluctuating and quickly decaying population activity (Fig. 1F, Fig. 4C) show that the corresponding population eigenvalue (Fig. 4A, yellow dot) is negative, the feedback is inhibition dominated and the network is said to be dynamically balanced ([5, 6, 19], Fig. 4, Case 1).

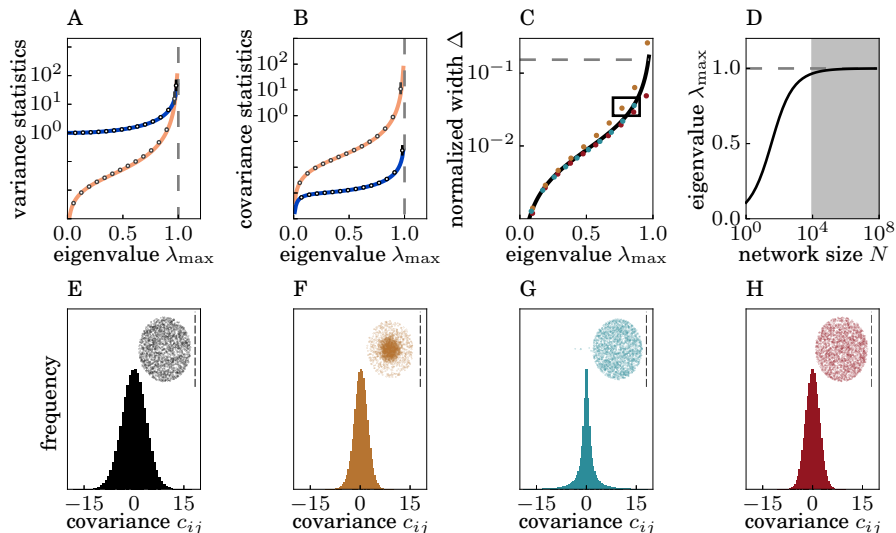


Figure 3. **Large relative dispersion of covariances reveals dynamics of motor cortex close to instability.** (A)-(B) Theoretical prediction for the mean (Eq. (2), blue curve) and standard deviation (Eq. (3), orange curve) of variances (panel A) and covariances (panel B) for different maximum eigenvalues  $\lambda_{\max}$  compared to numerical results (Eq. 1, markers) for homogeneous inhibitory networks. Ensemble averages for 100 network realizations (circles), average upward/downward deviation of the non-Gaussian statistics (bars). Bars are below marker size except for rightmost data points. (C) Theoretical prediction for the normalized width  $\Delta$  (black curve) of covariances compared to numerical results (Eq. 1, markers) for excitatory-inhibitory networks (yellow), inhibitory networks with distance-dependent connectivity (cyan), and numerical simulations of inhibitory networks of spiking leaky integrate-and-fire neurons (red). Distributions corresponding to data points within the black rectangle are shown in panels E-H. (D) Predicted maximum eigenvalue  $\lambda_{\max}$  (Eq. 4) of the effective connectivity as a function of the number of neurons  $N$  for given moments of the covariance distribution measured in macaque motor cortex ( $\Delta = 0.15$ , Fig. 1D). The shaded area marks the range of biologically plausible effective network sizes corresponding to the spatial scale of the recordings. (E)-(H) Distribution of covariances (histogram) and bulk eigenvalues (dots) relative to the critical line  $\text{Re}(\lambda_{\max}) = 1$  (dashed black line) for a homogeneous inhibitory network model (panel E), for a network of excitatory and inhibitory neurons (panel F), for a network with distance-dependent connection probability (G), and for a network of spiking leaky integrate-and-fire neurons (panel H).

This operational regime is in contrast to avalanche criticality [20] in networks with equal excitatory and inhibitory feedback ( $\mu \approx 1/N$ , Fig. 4, Case 2). The strongly fluctuating population activity observed in such networks causes positive covariances (Fig 4E) and a slowly decaying autocorrelation function of the population activity (Fig. 4F). These dynamics are determined by the single, nearly unstable eigenvalue of the population activity that results from the average connectivity structure of the network [21] (Fig 4D, yellow dot). Each of the remaining  $N - 1$  modes has a low amplitude and an exponentially decaying, fast dynamics (Fig. 4F). The network in such a critical state is hence effectively one-dimensional [22].

The high-dimensional criticality found here is not necessarily specific to macaque motor cortex. Experimental evidence for the operation of cortical networks in the dynamically balanced state is overwhelming [23–25]. In addition to the low average covariances in this state, other cortical areas, such as visual cortex [26], also show a covariance dispersion comparable to our data [18]. The same analysis applied to different cortical areas and experimental conditions can be used to determine their operational point  $\lambda_{\max}$ .

The operation in the dynamically balanced, critical regime ( $\lambda_{\max} \lesssim 1$ ) suggests several implications for learning and information processing. Neurons belonging to a critical mode show pairwise covariances that strongly exceed the average (Fig. 4B). Such covariances are likely to interact with spike-timing dependent synaptic plasticity [27, 28], leading to an increased interaction between neuronal and synaptic dynamics. Weak external inputs to the network are, moreover, sufficient to shift a large number of eigenvalues across the edge of stability [9], and thereby drastically change the recurrent network dynamics. Critical modes have a multitude of characteristic shapes and life times (Fig. 4C inset, [29]); they arise here despite the stereotypical and fast dynamics of individual neurons as a result of the heterogeneity of the network. The rich repertoire enables the parallel integration and maintenance of signals over prolonged time scales. Such networks provide a wealth of transformations on the input and therefore may serve as an exhaustive reservoir for computation [30, 31].

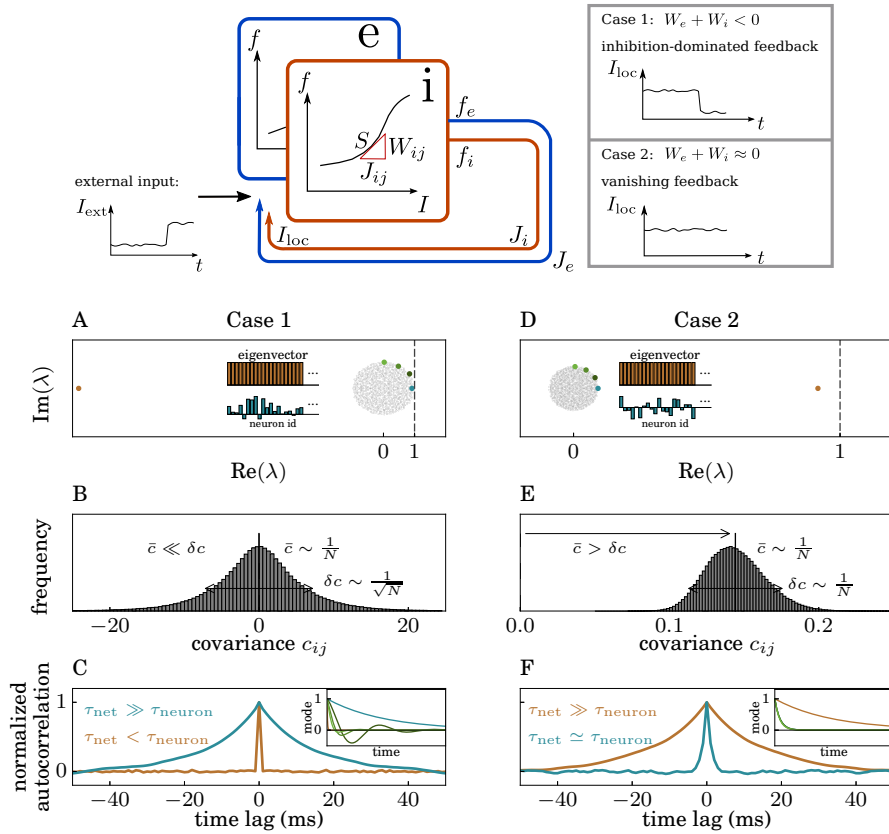


Figure 4. **Two types of criticality.** **Top:** Classification of networks based on feedback of population activity. A perturbation by an external input  $\delta I_{\text{ext}}$  (black time course) to an excitatory (blue) and inhibitory (red) population of neurons causes changes in firing rates  $\delta f = S \cdot \delta I_{\text{ext}}$  and recurrent inputs  $\delta I_{\text{loc}} = J_e \delta f_e + J_i \delta f_i = (W_e + W_i) \delta I_{\text{ext}}$  via excitatory ( $J_e$ , blue arrow) and inhibitory ( $J_i$ , red arrow) local connections. The recurrent input either counteracts the change in the external input (Case 1, inhibition-dominated feedback, top gray box), remains unaffected (Case 2, vanishing feedback, bottom gray box) or amplifies the external perturbation (locally unstable, not shown). **Bottom:** Resulting activity statistics on the level of individual neurons in cases 1 and 2, respectively, in the critical regime. Case 1 (left): Dynamically balanced network with stable population activity but virtually unstable linearized dynamics hidden in specific linear combinations of neuron activities. **(A)** Spectrum of eigenvalues with negative outlier (yellow dot) and nearly critical bulk eigenvalue (cyan dot) and corresponding eigenvector (cyan bars) generated by heterogeneity in connections across neuron pairs. **(B)** Distribution of covariances with almost vanishing mean and large standard deviation. **(C)** Autocorrelation functions of the population activity (yellow curve, cf. yellow dot in panel A) and the activity projected onto the eigenvector corresponding to the largest real bulk eigenvalue (cyan curve). Inset: Time course of network modes corresponding to colored eigenvalues in panel A. Case 2 (right): Network with almost vanishing excitatory and inhibitory feedback and virtually unstable linearized population dynamics. **(D)** Spectrum of eigenvalues with positive outlier (yellow dot) and corresponding eigenvector (yellow bars, population activity) generated by average connectivity structure. **(E)** Distribution of covariances with positive mean and small standard deviation. **(F)** Autocorrelation functions of the population activity (yellow curve) and the activity projected onto the eigenvector corresponding to the largest bulk eigenvalue (cyan curve, cf. cyan dot in panel D). Inset: Time course of network modes corresponding to colored eigenvalues in panel D.

Finally, the two types of criticality are not mutually exclusive as they are governed by different mechanisms. They can coexist in different brain regions or even in the same local network; networks may hence dynamically be moved into either regime to adapt brain function to momentary demands.

#### ACKNOWLEDGMENTS

We are grateful to Alexa Riehle and Thomas Brochier for providing the experimental data. We thank Vahid Rostami for help with the analysis of the multi-channel data. The research was carried out within the scope of the International Associated Laboratory “Vision for Action - LIA V4A“ of INT (CNRS, AMU), Marseilles and INM-6, Jülich. This

work was partially supported by HGF young investigator's group VH-NG-1028, Helmholtz portfolio theme SMHB, and EU Grants 604102 and 720270 (Human Brain Project, HBP).

- 
- [1] W. L. Shew and D. Plenz, *Neuroscientist* **19**, 88 (2013).
- [2] J. M. Beggs and D. Plenz, *J. Neurosci.* **23**, 11167 (2003).
- [3] T. Petermann, T. C. Thiagarajan, M. A. Lebedev, M. A. Nicolelis, D. R. Chialvo, and D. Plenz, *Proc. Nat. Acad. Sci. USA* **106**, 15921 (2009).
- [4] C. van Vreeswijk and H. Sompolinsky, *Science* **274**, 1724 (1996).
- [5] A. Renart, J. De La Rocha, P. Bartho, L. Hollender, N. Parga, A. Reyes, and K. D. Harris, *Science* **327**, 587 (2010).
- [6] T. Tetzlaff, M. Helias, G. Einevoll, and M. Diesmann, *PLOS Comput. Biol.* **8**, e1002596 (2012).
- [7] A. Riehle, S. Wirtsohn, S. Grün, and T. Brochier, *Frontiers in Neural Circuits* **7**, 48 (2013), doi: 10.3389/fncir.2013.00048.
- [8] N. Bertschinger and T. Natschläger, *Neural Comput.* **16**, 1413 (2004).
- [9] G. Wainrib and J. Touboul, *Phys. Rev. Lett.* **110**, 118101 (2013).
- [10] H. Sompolinsky, A. Crisanti, and H. J. Sommers, *Phys. Rev. Lett.* **61**, 259 (1988).
- [11] B. Lindner, B. Doiron, and A. Longtin, *Phys. Rev. E* **72**, 061919 (2005).
- [12] V. Pernice, B. Staude, S. Cardanobile, and S. Rotter, *PLOS Comput. Biol.* **7**, e1002059 (2011).
- [13] J. Trousdale, Y. Hu, E. Shea-Brown, and K. Josic, *PLOS Comput. Biol.* **8**, e1002408 (2012).
- [14] C. Chow and M. Buice, *The Journal of Mathematical Neuroscience* **5** (2015).
- [15] C. De Dominicis, *Phys. Rev. B* **18**, 4913 (1978).
- [16] H. Sompolinsky and A. Zippelius, *Phys. Rev. B* **25**, 6860 (1982).
- [17] M. Moshe and J. Zinn-Justin, *Physics Reports* **385**, 69 (2003), ISSN 0370-1573.
- [18] *See supplementary material.*
- [19] M. R. Cohen and A. Kohn, *Nat. Rev. Neurosci.* **14**, 811 (2011), doi:10.1038/nrn.2842.
- [20] G. Tkacik, T. Mora, O. Marre, D. Amodei, S. E. Palmer, M. J. Berry, and W. Bialek, *Proc. Nat. Acad. Sci. USA* **112**, 11508 (2015).
- [21] D. B. Larremore, W. L. Shew, and J. G. Restrepo, *Phys. Rev. Lett.* **106**, 058101 (2011).
- [22] G. Tkacik, O. Marre, D. Amodei, E. Schneidman, W. Bialek, and M. J. Berry II, *PLoS Comp Biol* **10**, e1003408 (2014).
- [23] M. Okun and I. Lampl, *Nat. Neurosci.* **11**, 535 (2008).
- [24] K. Reinhold, A. D. Lien, and M. Scanziani, *Nat. Neurosci.* **18**, 1789 (2015).
- [25] N. Dehghani, A. Peyrache, B. Telenczuk, M. Le Van Quyen, E. Halgren, S. S. Cash, N. G. Hatsopoulos, and A. Destexhe, *Scientific reports* **6** (2016).
- [26] A. S. Ecker, P. Berens, G. A. Keliris, M. Bethge, and N. K. Logothetis, *Science* **327**, 584 (2010).
- [27] H. Markram, J. Lübke, M. Frotscher, and B. Sakmann, *Science* **275**, 213 (1997).
- [28] A. Morrison, M. Diesmann, and W. Gerstner, *Biol. Cybern.* **98**, 459 (2008).
- [29] G. Hennequin, T. Vogels, and W. Gerstner, *Neuron* **82**, 1394 (2014).
- [30] W. Maass, T. Natschläger, and H. Markram, *Neural Comput.* **14**, 2531 (2002).
- [31] H. Jaeger and H. Haas, *Science* **304**, 78 (2004).
- [32] J. Aljadeff, M. Stern, and T. Sharpee, *Phys. Rev. Lett.* **114**, 088101 (2015).
- [33] J. Kadmon and H. Sompolinsky, *Phys. Rev. X* **5**, 041030 (2015).
- [34] D. Grytskyy, T. Tetzlaff, M. Diesmann, and M. Helias, *Front. Comput. Neurosci.* **7**, 131 (2013).
- [35] I. Ginzburg and H. Sompolinsky, *Phys. Rev. E* **50**, 3171 (1994).
- [36] M. Helias, T. Tetzlaff, and M. Diesmann, *PLOS Comput. Biol.* **10**, e1003428 (2014).
- [37] J. A. Hertz, Y. Roudi, and P. Sollich, *Journal of Physics A: Mathematical and Theoretical* **50**, 033001 (2017).
- [38] K. H. Fischer and J. A. Hertz, *Spin Glasses* (Cambridge University Press, 1991), ISBN 9780511628771.
- [39] C. W. Gardiner, *Handbook of Stochastic Methods for Physics, Chemistry and the Natural Sciences* (Springer-Verlag, Berlin, 1985), 2nd ed., ISBN 3-540-61634-9, 3-540-15607-0.
- [40] D. Sherrington and S. Kirkpatrick, *Phys. Rev. Lett.* **35**, 1792 (1975).
- [41] C. De Dominicis and L. Peliti, *Phys. Rev. B* **18**, 353 (1978).
- [42] H. Nishimori, *Statistical Physics of Spin Glasses and Information Processing An Introduction* (Clarendon Press, Oxford, 2001).
- [43] C. W. Gardiner, *Handbook of Stochastic Methods for Physics, Chemistry and the Natural Sciences* (Springer-Verlag, Berlin, 1983).
- [44] C. van Vreeswijk and H. Sompolinsky, *Neural Comput.* **10**, 1321 (1998).
- [45] D. J. Amit, *Field Theory, the Renormalization Group, and Critical Phenomena; 3rd ed.* (World Scientific, Singapore, 2005).
- [46] Y. Roudi and J. Hertz, *Physical Review Letters* **106**, 048702 (2011).
- [47] R. Barlow, *Statistics: A Guide to the Use of Statistical Methods in the Physical Sciences* (John Wiley & Sons, 2013).
- [48] E. L. Lehmann and G. Casella, *Theory of point estimation* (Springer Science & Business Media, 2006).

# Supplementary Materials

## I. MEAN-FIELD THEORY FOR META-STATISTICS BEYOND SELF-AVERAGING

Mean-field theory most-commonly employs the thermodynamic limit ( $N \rightarrow \infty$ ), reducing the collective dynamics of the  $N$  interacting units to  $N$  pairwise independent units, each subject to a self-consistently determined auxiliary field [4, 10, 32, 33]. Covariances of individual neurons are self-averaging in this limit, so they are identical for all units and independent of the realization of the randomness in the network connectivity. In particular, cross-covariances vanish. In the absence of external stimuli and in the weakly correlated regime, covariances can be understood in linear response theory [34]. For such a linearized network model, interactions between neurons can be included as a finite-size correction within this self-averaging framework [5, 6, 13, 35, 36]. While this procedure yields covariances averaged over many pairs of units, the experimentally observed neuron to neuron variability [26] is lost. Here, we develop a theory beyond self-averaging covariances that captures their statistics. It exploits the large size of biologically realistic local networks, but includes finite-size fluctuations of auxiliary fields which derive from the quenched disorder of the couplings to explain the variability of covariances. To perform this qualitative step, we need to combine methods from different fields: We use a functional formulation of Gaussian processes that originates from statistical field theory [14, 15, 37] and combine it with methods typically used for disordered systems in the large  $N$  limit [17], such as spin glasses [16, 38]. We outline these steps in detail below.

### A. Moment generating functional for the network dynamics

In the following, we consider time-lag integrated covariances

$$c_{ij} = \int_{-\infty}^{\infty} c_{ij}(\tau) d\tau = \int_{-\infty}^{\infty} \int_{-\infty}^{\infty} \langle x_i(t+\tau)x_j(t) \rangle_x dt d\tau = \langle X_i(0)X_j(0) \rangle_x, \quad (5)$$

calculated as averages  $\langle \rangle_x$  across different trials of the linearized network dynamics  $x(t)$  or its Fourier transform  $X(\omega)$  evaluated at  $\omega = 0$  (Wiener-Khinchin theorem, [39, sec. 1.4.2]). The linearized dynamics can be modeled as a set of coupled Ornstein-Uhlenbeck processes

$$\tau \frac{dx(t)}{dt} = -x(t) + W \cdot x(t) + \xi(t) \quad (6)$$

with the moment-generating functional

$$Z[j] = \int \mathcal{D}x \int \mathcal{D}\tilde{x} \exp\left(S_0[x, \tilde{x}] + j^T x\right) \\ \text{with } S_0[x, \tilde{x}] = \tilde{x}^T (\partial_t + 1 - W) x + \frac{D}{2} \tilde{x}^T \tilde{x}. \quad (7)$$

Here  $\xi(t)$  is a Gaussian white noise with variance  $\langle \xi_i(t)\xi_j(t') \rangle = D\delta_{ij}\delta(t-t')$ ,  $\tilde{x}(t)$  is a purely imaginary response field,  $\int \mathcal{D}\tilde{x}$ ,  $\int \mathcal{D}x$  are suitably defined path integral measures, and  $\tilde{x}^T \tilde{x} = \sum_i \int \tilde{x}_i(t) \tilde{x}_i(t) dt$  is a scalar product [14, 15, 37]. The generating functional can easily be interpreted in Fourier domain due to the linearity of Eq. (6) and the invariance of scalar products under unitary transforms

$$Z[J] = \int \mathcal{D}X \int \mathcal{D}\tilde{X} \exp\left(S_0[X, \tilde{X}] + J^T X\right) \\ \text{with } S_0[X, \tilde{X}] = \tilde{X}^T (i\omega + 1 - W) X + \frac{D}{2} \tilde{X}^T \tilde{X}, \quad (8)$$

with Fourier transformed variables denoted by capital letters. The scalar product in frequency domain reads  $\tilde{X}^T X = \sum_i \int \tilde{X}_i(-\omega)X_i(\omega) d\omega$ . The generating functional factorizes into generating functions for each frequency  $\omega$ . As shown in Eq. (5), time-lag integrated covariances only require the knowledge of  $X(0)$ . In the following, we will therefore only discuss zero frequency. After integration over all non-zero frequencies one obtains the generating function for

zero frequency

$$\begin{aligned} Z(J) &= \det(1 - W) \int \mathcal{D}X \int \mathcal{D}\tilde{X} \exp\left(S_0(X, \tilde{X}) + J^T X\right) \\ &= \exp\left(\frac{1}{2} J^T (1 - W)^{-1} D (1 - W^T)^{-1} J\right) \end{aligned} \quad (9)$$

$$\text{with } S_0(X, \tilde{X}) = \tilde{X}^T (1 - W) X + \frac{D}{2} \tilde{X}^T \tilde{X}, \quad (10)$$

with the single-frequency ( $\omega = 0$ ) scalar product defined as  $\tilde{X}^T X = \sum_i \tilde{X}_i X_i$ , and integration measures  $\int \mathcal{D}X = \prod_j \int_{-\infty}^{\infty} dX_j$  and  $\int \mathcal{D}\tilde{X} = \prod_j \frac{1}{2\pi i} \int_{-\infty}^{\infty} d\tilde{X}_j$ . The determinant in Eq. (9) follows from the normalization condition  $Z[J=0] = 1$ . The time-lag integral of the covariance functions follows as

$$c(W) = [1 - W]^{-1} D [1 - W^T]^{-1}. \quad (11)$$

## B. Self-averaging meta-statistics

Equation (11) relates covariances between individual pairs of neurons to the connectivity matrix  $W$ . These, however, change between realizations of the random connectivity. In contrast, the meta-statistics, by which we denote the moments of the distribution of covariances, can be assumed constant across realizations (self-averaging, [38]). We therefore seek for an expression relating the moments of the distribution of covariances to the statistics of the connectivity  $W$ .

We denote with  $\bar{\cdot}$  the empirical average, with  $\langle \cdot \rangle_x$  the expectation over realizations of the processes  $x$ , and with  $\langle \cdot \rangle$  the ensemble average over the disordered connectivity  $W$ . Exchanging the order of differentiation and averaging allows expressing second moments of covariances as derivatives of a single disorder-averaged generating function  $\langle Z(J) \rangle$ : We first assume the empirical average to be self-averaging

$$\bar{c}_{ii}^2 = \langle \bar{c}_{ii}^2 \rangle. \quad (12)$$

We then use its definition as  $\bar{c}_{ii}^2 = \frac{1}{N} \sum_{i=1}^N c_{ii}^2$ , and that of the second cumulant  $c_{ij} = \langle X_i X_j \rangle_x$  of the zero frequency components  $X = X(\omega = 0) = \int_{-\infty}^{\infty} x(t) dt$  of Ornstein-Uhlenbeck processes  $x$  to obtain

$$\bar{c}_{ii}^2 = \frac{1}{N} \sum_{i=1}^N \langle \langle X_i X_i \rangle_x^2 \rangle. \quad (13)$$

As the action Eq. (9) for a single realization of  $W$  is quadratic, Wick's theorem applies,  $\langle X_i X_i X_j X_j \rangle_x = 2 \langle X_i X_j \rangle_x^2 + \langle X_i X_i \rangle_x \langle X_j X_j \rangle_x = 2c_{ij}^2 + c_{ii}c_{jj}$  for the special case  $i = j$ , such that we may identify the squared second moment (13) with a fourth moment. The latter can be expressed with the help of the generating function

$$\begin{aligned} \bar{c}_{ii}^2 &= \frac{1}{N} \sum_{i=1}^N \langle \langle X_i X_i \rangle_x^2 \rangle \stackrel{\text{Wick's th.}}{=} \frac{1}{N} \sum_{i=1}^N \frac{1}{3} \langle \langle X_i X_i X_i X_i \rangle_x \rangle \\ &= \frac{1}{N} \sum_{i=1}^N \frac{1}{3} \left\langle \frac{d^4}{dJ_i^4} Z(J) \right\rangle \Big|_{J=0} = \frac{1}{3} \frac{d^4}{dJ_i^4} \langle Z(J) \rangle \Big|_{J=0}. \end{aligned} \quad (14)$$

In the last step, we exchanged the order of derivatives and the expectation value over network realizations and used the symmetry of the disorder-averaged network over units. Analogously follows for  $i \neq j$  and  $N - 1 \approx N$ ,

$$\bar{c}_{ij}^2 = \frac{1}{2} \frac{d^4}{dJ_i^2 dJ_j^2} \langle Z(J) \rangle \Big|_{J=0} - \frac{1}{2} \langle \bar{c}_{ii} \rangle^2. \quad (15)$$

### C. Disorder-averaged generating function

Ignoring insignificant variations in the normalization  $\det(1 - W)$  of  $Z[J]$ , the disorder average only affects the coupling term in Eq. (9)

$$\begin{aligned} \langle \exp(\tilde{X}^T W X) \rangle &= \left\langle \exp \left( \sum_{i,j} W_{ij} \tilde{X}_i X_j \right) \right\rangle \\ &= \prod_{i,j} \langle \exp(W_{ij} \tilde{X}_i X_j) \rangle \\ &= \prod_{i,j} \exp \left( \sum_{k=1}^{\infty} \frac{\kappa_k}{k!} (\tilde{X}_i X_j)^k \right). \end{aligned}$$

For clarity, we here assume independent and identically distributed weights  $W_{ij}$ . In the resulting cumulant expansion [38, 40–42]  $\kappa_k$  is the  $k$ -th cumulant for a single connection  $W_{ij}$  [43]. For fixed connection probability  $p$ , the number of inputs to a neuron scales with the network size  $N$ . To keep the input and its fluctuations within a certain dynamic range when increasing the network size, we require synaptic weights to scale with  $1/\sqrt{N}$  [4, 44], such that the cumulant expansion is an expansion in  $1/\sqrt{N}$ . A truncation at the second cumulant ( $\propto N^{-1}$ ) maps  $W$  to a Gaussian connectivity  $\mathcal{N}(\mu, \lambda_{\max}^2/N)$  so that

$$\begin{aligned} \langle Z(J) \rangle &\sim \int \mathcal{D}X \int \mathcal{D}\tilde{X} \exp \left( S_0(X, \tilde{X}) + \frac{\lambda_{\max}^2}{2N} V(X, \tilde{X}) + J^T X \right), \quad (16) \\ S_0(X, \tilde{X}) &= \tilde{X}^T (1 - \mu) X + \frac{D}{2} \tilde{X}^T \tilde{X}, \\ V(X, \tilde{X}) &= \tilde{X}^T \tilde{X} X^T X, \end{aligned}$$

with a homogeneous mean connection weight  $\mu_{ij} = \mu = \mathcal{O}(1/\sqrt{N})$ . The second cumulant ( $\lambda_{\max}^2/N$ ) is the first non-trivial contribution to the second moment of covariances. While higher cumulants of the connectivity have an impact on higher moments of the distribution of covariances, their effect on the first two moments is suppressed by the large network size.

### D. Auxiliary-field formalism

The interaction term  $V$  prevents an exact calculation of the disorder-averaged generating function. A converging perturbation series can be obtained in the auxiliary-field formulation [17], where a field  $Q_1 = \frac{\lambda_{\max}^2}{N} X^T X$  is introduced for the sum of a large number of statistically equivalent activity variables. Using the Hubbard-Stratonovich transformation

$$\begin{aligned} e^{\frac{\lambda_{\max}^2}{2N} \tilde{X}^T \tilde{X} X^T X} &= \int_{-\infty}^{\infty} dQ_1 \delta \left( Q_1 - \frac{\lambda_{\max}^2}{N} X^T X \right) e^{\frac{1}{2} Q_1 \tilde{X}^T \tilde{X}} \\ &= \underbrace{\frac{1}{2\pi i} \frac{N}{\lambda_{\max}^2} \int_{-\infty}^{\infty} dQ_1 \int_{-i\infty}^{i\infty} dQ_2}_{\int \mathcal{D}Q} e^{-\frac{N}{\lambda_{\max}^2} Q_1 Q_2 + \frac{1}{2} Q_1 \tilde{X}^T \tilde{X} + Q_2 X^T X}, \end{aligned}$$

one obtains a free theory, which is a quadratic action in the activity ( $X$ ) and response variables ( $\tilde{X}$ ), on the background of fluctuating fields  $Q$

$$\begin{aligned} \langle Z(J) \rangle &\sim \int \mathcal{D}Q \exp \left( -\frac{N}{\lambda_{\max}^2} Q_1 Q_2 + \ln(Z_Q(J)) \right), \quad (17) \\ Z_Q(J) &= \int \mathcal{D}X \int \mathcal{D}\tilde{X} \exp \left( S_0(X, \tilde{X}) + \frac{1}{2} Q_1 \tilde{X}^T \tilde{X} + Q_2 X^T X + J^T X \right). \end{aligned}$$

The high dimensional integrals of the free theory  $Z_Q(J)$  can be solved analytically yielding a two-dimensional interacting theory in the auxiliary fields  $Q_1$  and  $Q_2$ . The auxiliary field formalism translates the high-dimensional ensemble average over  $W$  to a low-dimensional average over  $Q$ ; it maps the local disorder in the connections to fluctuations

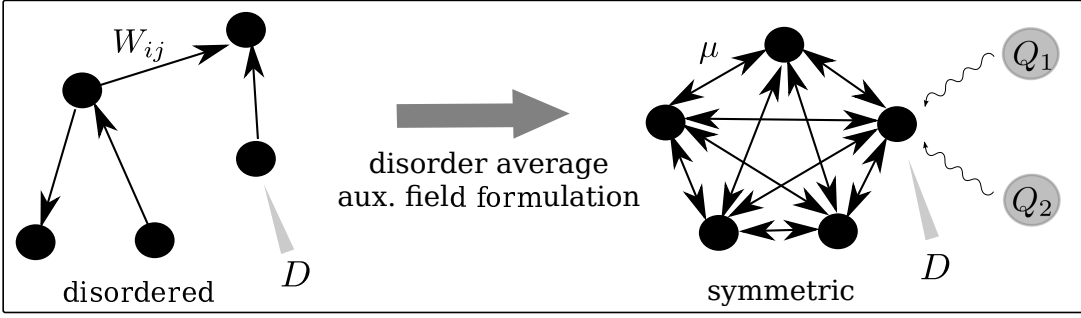


Figure S1. **Reduction of a disordered to a regular network.** Disorder average maps network with frozen variability in connections (left) to highly symmetric network on the background of fluctuating auxiliary fields  $Q$  (right). Their fluctuations contribute globally to the covariance that drives the network fluctuations (illustrated by wavy arrows).

of global fields  $Q$  interacting with a highly symmetric all-to-all connected network, illustrated in Fig. S1. Only in the special case of vanishing mean connection strength  $\mu = 0$ , the system factorizes into  $N$  unconnected units, each interacting with the same set of fields  $Q$ . The all-to-all network not only captures the autocovariance of a single neuron, but also the cross-covariance with any other neuron.

### E. Saddle-point approximation

Performing a change of variables  $Q = Q^*(J) + \frac{\delta Q}{\sqrt{N}}$  in Eq. (17), where  $Q^*(J)$  are the saddle-points of the exponent  $-\frac{N}{\lambda_{\max}^2} Q_1 Q_2 + \ln(Z_Q(J)) =: -N \cdot Y(Q_1, Q_2, J)$  determined by the saddle-point equations

$$0 = \left. \frac{\partial}{\partial Q_\alpha} Y(Q_1, Q_2, J) \right|_{Q=Q^*(J)} \quad \alpha \in \{1, 2\}, \quad (18)$$

and expanding  $Y(Q_1, Q_2, J)$  around  $Q^*(J)$ , yields an expansion in powers of  $1/N$  [17, 45]. We focus only on the leading-order contribution  $Y(Q_1^*(J), Q_2^*(J), J)$  which describes tree-level diagrams in the  $Q$ -theory and drop all source dependence in higher Taylor coefficients

$$\langle Z(J) \rangle \sim \exp(-N \cdot Y(Q_1^*(J), Q_2^*(J), J)), \quad (19)$$

with the corresponding action

$$S_{Q_\alpha^*(J)}(X, \tilde{X}) = \tilde{X}^T (1 - \mu) X + \frac{D + Q_1^*(J)}{2} \tilde{X}^T \tilde{X} + Q_2^*(J) X^T X. \quad (20)$$

Note that this Gaussian theory in  $X, \tilde{X}$  still contains in the latter two terms contributions from the quartic interaction term  $V$  of the original theory. Variability in  $Q^*(J)$ , through their source dependence, therefore gives rise to cumulants of the activity variables beyond second order. The dependence of  $Q^*(J)$  on external sources  $J$  was neglected in prior work [16] since it scales to leading order as  $1/N$ . This approximation, however, yields a Gaussian theory (see Eq. (20) for  $J = 0$ ), which does not generate fourth cumulants and therefore no distribution of covariances. Taking into account the  $J$  dependence of auxiliary fields in combination with the relation between fourth cumulants and distributions of covariances Eq. (14) and Eq. (15) thus extends mean-field theory beyond self-averaging covariances.

The action (20) shows that  $Q_1^*(J)$  acts as a global contribution to the Gaussian noise whereas  $Q_2^*(J)$  directly contributes to the inverse of the covariance matrix. By integrating out the response variables  $\tilde{X}$ , one can alternatively interpret both  $Q_\alpha^*(J)$  as contributions to the covariance matrix of the noise.

Saddle points  $Q^*(J)$  are obtained self-consistently from Eq. (18) which reduces to the set of equations

$$\begin{aligned} Q_1^*(J) &= \frac{\lambda_{\max}^2}{N} \langle X^T X \rangle_{Q_\alpha^*(J)}(J) \\ Q_2^*(J) &= \frac{\lambda_{\max}^2}{2N} \langle \tilde{X}^T \tilde{X} \rangle_{Q_\alpha^*(J)}(J) \end{aligned} \quad (21)$$

with  $\langle \circ \rangle_{Q_\alpha^*(J)}(J) := \frac{\int \mathcal{D}X \int \mathcal{D}\tilde{X} \circ \exp(S_{Q_\alpha^*(J)}(X, \tilde{X}) + J^T X)}{\int \mathcal{D}X \int \mathcal{D}\tilde{X} \exp(S_{Q_\alpha^*(J)}(X, \tilde{X}) + J^T X)}$

The above set of equations cannot be solved analytically for  $Q^*(J)$ . However, moments of activity result from derivatives of  $\langle Z(J) \rangle$  evaluated at  $J = 0$ . The derivatives act not only on the source term  $J^T X$ , but also on the  $J$ -dependence of the saddle-point. Therefore, moments are determined by saddle-points and their derivatives evaluated at zero source. Setting  $J = 0$  in Eq. (21) yields the self-consistent result

$$\langle \tilde{X}_i \tilde{X}_j \rangle_{Q_\alpha^*} = 0, \quad (22)$$

$$\langle X_i X_j \rangle_{Q_\alpha^*} = \left[ (1 - \mu)^{-1} (D + Q_1^*) (1 - \mu^T)^{-1} \right]_{ij}, \quad (23)$$

$$\langle \tilde{X}_i X_j \rangle_{Q_\alpha^*} = \left[ (1 - \mu)^{-1} \right]_{ij}, \quad (24)$$

with

$$Q_1^* := Q_1^*(0) = \frac{R^2}{1 - R^2} D, \quad (25)$$

$$Q_2^* := Q_2^*(0) = 0,$$

$\langle \circ \rangle_{Q_\alpha^*} := \langle \circ \rangle_{Q_\alpha^*(0)}$ ,  $R = \sqrt{1 + \gamma} \lambda_{\max} \approx \lambda_{\max}$  and  $\gamma = \mathcal{O}(1/N)$  resulting from subleading terms in Eq. (23) containing  $\mu$ . Eq. (23) shows that  $Q_1^*$  leads to a renormalization of the noise  $D$  as  $D_\lambda = D + Q_1^* = D/(1 - R^2) \approx D/(1 - \lambda_{\max}^2)$ .

Analogously, second derivatives of saddle-points with respect to sources can be calculated from Eq. (21) with the final result

$$\begin{aligned} \left. \frac{d^2 Q_1^*(J)}{dJ_k dJ_l} \right|_{J=0} &= \frac{\lambda_{\max}^2}{\beta N} \sum_i \langle X_i X_k \rangle_{Q_\alpha^*} \langle X_i X_l \rangle_{Q_\alpha^*} + \frac{\lambda_{\max}^2}{\beta N} \sum_{i,a} \langle X_i X_a \rangle_{Q_\alpha^*}^2 \left. \frac{d^2 Q_2^*(J)}{dJ_k dJ_l} \right|_{J=0}, \\ \left. \frac{d^2 Q_2^*(J)}{dJ_k dJ_l} \right|_{J=0} &= \frac{\lambda_{\max}^2}{\beta N} \sum_i \langle \tilde{X}_i X_k \rangle_{Q_\alpha^*} \langle \tilde{X}_i X_l \rangle_{Q_\alpha^*}, \quad \text{with } \beta = 1 - \frac{\lambda_{\max}^2}{N} \sum_{i,a} \langle X_i \tilde{X}_a \rangle_{Q_\alpha^*}^2, \end{aligned}$$

where we used that  $\left. \frac{dQ_\alpha^*(J)}{dJ_k} \right|_{J=0} = 0$  since three-point correlators vanish.

Using partial derivative calculus  $\frac{d}{dJ_i} \langle Z(J) \rangle = \left( \frac{\partial Q_1^*}{\partial J_i} \frac{\partial}{\partial Q_1^*} + \frac{\partial Q_2^*}{\partial J_i} \frac{\partial}{\partial Q_2^*} + \frac{\partial}{\partial J_i} \right) \langle Z(Q_1^*, Q_2^*, J) \rangle$  and the saddle-point condition  $\frac{\partial}{\partial Q_\alpha^*} \langle Z(Q_1^*, Q_2^*, J) \rangle = 0$  which follows from Eq. (18) and Eq. (19), we find that second moments of activity, the average covariances, are not influenced by the source dependence of saddle points

$$\langle \langle X_i X_j \rangle_x \rangle = \left. \frac{d^2}{dJ_i dJ_j} \langle Z(J) \rangle \right|_{J=0} = \langle X_i X_j \rangle_{Q_\alpha^*} = \left[ (1 - \mu)^{-1} D_\lambda (1 - \mu^T)^{-1} \right]_{ij}. \quad (26)$$

The non-zero mean connection strength  $\mu = \mathcal{O}(1/\sqrt{N})$  yields cross-covariances between neurons due to the finite size of the network. In addition, the fourth moments of activity are crucial for the non-vanishing variance of covariances: Formally, two of the four derivatives act on  $Q^*(J)$  while the other two act on the source term  $J^T X$  to yield

$$\begin{aligned} \langle \langle X_i X_j X_i X_j \rangle_x \rangle &= \left. \frac{d^4}{dJ_i dJ_j dJ_i dJ_j} \langle Z(J) \rangle \right|_{J=0} \\ &= 4 \left. \frac{d^2 Q_1^*(J)}{dJ_i dJ_j} \right|_{J=0} \sum_a \langle X_i \tilde{X}_a \rangle_{Q_\alpha^*} \langle X_j \tilde{X}_a \rangle_{Q_\alpha^*} + 2 \left. \frac{d^2 Q_1^*(J)}{dJ_i dJ_i} \right|_{J=0} \sum_a \langle X_j \tilde{X}_a \rangle_{Q_\alpha^*} \langle X_j \tilde{X}_a \rangle_{Q_\alpha^*} \\ &+ 4 \left. \frac{d^2 Q_2^*(J)}{dJ_i dJ_j} \right|_{J=0} \sum_a \langle X_i X_a \rangle_{Q_\alpha^*} \langle X_j X_a \rangle_{Q_\alpha^*} + 2 \left. \frac{d^2 Q_2^*(J)}{dJ_i dJ_i} \right|_{J=0} \sum_a \langle X_j X_a \rangle_{Q_\alpha^*} \langle X_j X_a \rangle_{Q_\alpha^*} \\ &+ 2 \langle X_i X_j \rangle_{Q_\alpha^*} \langle X_i X_j \rangle_{Q_\alpha^*} + \langle X_i X_i \rangle_{Q_\alpha^*} \langle X_j X_j \rangle_{Q_\alpha^*}. \end{aligned} \quad (27)$$

The latter two terms in Eq. (27) correspond to the trivial Wick decomposition from the Gaussian part of the theory at  $Q_\alpha^* = Q_\alpha^*(J = 0)$ , whereas the second derivatives of saddle points  $\left. \frac{d^2 Q_\alpha^*(J)}{dJ_i dJ_j} \right|_{J=0} = \mathcal{O}(1/N)$  evaluated at zero source determine the non-vanishing fourth cumulants. Note that no quartic derivatives of saddle points appear in Eq. (27) due to the saddle-point condition  $\frac{\partial}{\partial Q_\alpha^*} \langle Z(Q_1^*, Q_2^*, J) \rangle = 0$ .

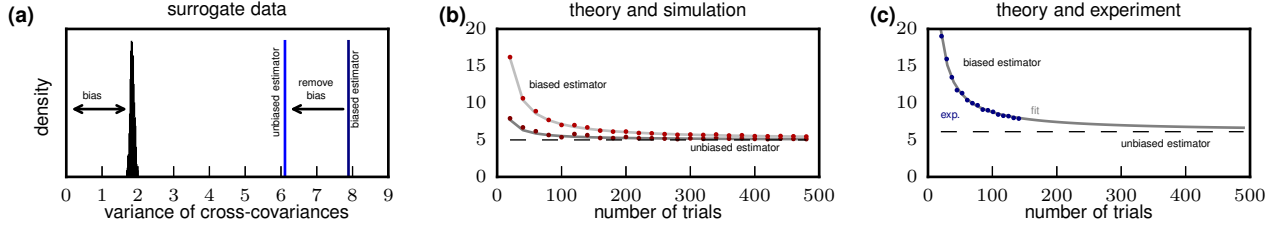


Figure S2. **Assessment and correction of the bias in estimator of variance of cross-covariances.** (a) Variance of cross-covariances (black distribution) obtained from trial-shuffled data compared to the biased estimator (Eq. (33), dark blue) and unbiased estimator (light blue) of the true variance as obtained from experimental data. (b) Convergence of biased estimator for small (dark gray) and large (light gray) mean covariances towards true variance given by unbiased estimator (dashed line). Curves indicate the theoretical prediction Eq. (33), dots numerical simulations for artificial data. (c) True value 6.11 of variance of cross-covariances (dashed line) derived from fitting (gray curve) Eq. (33) to the biased estimator (blue dots) obtained from subsampled experimental data with different numbers of trials.

### F. Mean and variance of the covariance distribution

We obtain the mean integral covariances (see Eq. (26))

$$\overline{c_{ij}} = \left[ (1 - \mu)^{-1} D_\lambda (1 - \mu^T)^{-1} \right]_{ij} = D_\lambda \gamma_{ij} \quad (28)$$

and the variance of integral covariances (see Eq. (14), Eq. (15) and Eq. (27))

$$\overline{\delta c_{ij}^2} = \lambda_{\max}^2 \left[ \frac{1}{(1 - \lambda_{\max}^2)^2} + \frac{1}{1 - \lambda_{\max}^2} \right] D_\lambda^2 \chi_{ij}. \quad (29)$$

The mean connectivity  $\mu$  enters the coefficients  $\gamma_{ij} = \delta_{ij} + \gamma$  (with  $\delta_{ij}$  the Kronecker symbol),  $\chi_{ij} = \frac{1}{N} (1 + \delta_{ij} + \mathcal{O}(1/N))$  and  $\gamma = \mathcal{O}(1/N)$  only in their sub-leading corrections, and acts as a negative feedback in inhibitory or inhibition-dominated networks [6]. While this feedback suppresses mean cross-covariances (28) which consequently scale as  $\overline{c_{ij}} \sim \frac{1}{N}$ , it only yields a subleading contribution to the dispersion (29). The spread of individual cross-covariances is determined by fluctuations in connection weights and shows a scaling as  $\sqrt{\overline{\delta c_{ij}^2}} \sim \frac{1}{\sqrt{N}}$ . These fluctuations, which formally originate from the variability of the auxiliary fields  $Q$ , are therefore much larger than the mean; they cause broad distributions of cross-covariances of both signs even in a homogeneous network. The expressions therefore explain the first two moments of the experimentally observed distribution of cross-covariances: mean cross-covariances scale as  $\mathcal{O}(1/N)$ , whereas the standard deviation only scales as  $\mathcal{O}(1/\sqrt{N})$ . The width of the distribution is thus much larger than the mean for large networks and the distribution is centered approximately around zero.

We note that this approach is inherently different from mean-field theories for single realizations of network connectivities which keep the site dependence to infer relations between covariances and connections on the level of individual neurons [46]. In contrast, we derive a relation between the statistics of the structure and the statistics of the dynamics using a quenched average. The crucial feature of the presented theory is that heterogeneity across neurons can still be extracted from the ensemble description. We here show that the heterogeneity is closely linked to fluctuations of the auxiliary fields, which are accessible by studying their source dependence.

## II. BIAS AND ERROR OF ESTIMATING THE DISPERSION IN EXPERIMENTAL DATA

Due to limited numbers of trials, the estimator for the dispersion of the covariance may be biased towards larger variances. We seek to find a correction for this bias, as illustrated in Fig. S2a. To this end we derive the dependence of experimentally estimated moments of the activities on the number of neurons and trials. The derivation here follows the standard approach of correcting the estimation, sometimes called Bessel's correction [47].

We assume a probability distribution  $p(n^1, \dots, n^{N_T})$ ,  $n^k \in \mathbb{N}_0^N$ , of activities  $n_i^k$  of neuron  $i$  in trial  $k \in \{1, \dots, N_T\}$ . We assume that the spike counts are sufficiently large so that their statistics is to leading order described by its first two cumulants, which is in line with our findings in Section I. We further assume that there are no correlations

between different trials, so that the probability distribution factorizes over trials and the moment generating function reads

$$\phi(l^1, \dots, l^{N_T}) = \prod_{k=1}^{N_T} \exp\left(m^T l^k + \frac{1}{2} l^{k,T} c l^k\right), \quad (30)$$

where  $m$  is the vector of mean activities with mean  $\overline{m}$  and variance  $\overline{\delta m^2}$  across neurons,  $c$  is the covariance matrix with mean autocovariance  $\overline{a}$ , variance of autocovariances  $\overline{\delta a^2}$ , mean cross-covariance  $\overline{c}$  and variance of cross-covariances  $\overline{\delta c^2}$  across neurons. The meta-statistics are assumed to be identical across trials. Furthermore, we assume the meta-statistics to be the same for all realizations of distributions of mean activities and covariances across neurons. In the following,  $\langle \rangle$  denotes the average over these realizations obtained from the averaged moment generating function

$$\begin{aligned} \langle \phi(l^1, \dots, l^{N_T}) \rangle &= \exp\left(\sum_{k=1}^{N_T} \left(\overline{m} \sum_i l_i^k + \frac{1}{2} \overline{a} \sum_i l_i^k l_i^k + \frac{1}{2} \overline{c} \sum_{i \neq j} l_i^k l_j^k\right)\right) \\ &+ \sum_{k,l=1}^{N_T} \left(\frac{1}{2} \overline{\delta m^2} \sum_i l_i^k l_i^l + \frac{1}{8} \overline{\delta a^2} \sum_i l_i^k l_i^k l_i^l l_i^l + \frac{1}{8} \overline{\delta c^2} \sum_{i \neq j} l_i^k l_j^k l_i^l l_j^l\right) \end{aligned} \quad (31)$$

and  $\hat{\cdot}$  denotes the empirical estimates of mean activities and covariances from  $N$  recorded neurons in  $N_T$  trials of the experiment. Note that the average across realizations formally introduces correlations between different trials (mixed  $k, l$  terms in (31)) which allow us to calculate corrections due to the finite number of trials. Using Eq. (31), it is straight-forward to show and well known that an empirical covariance defined as  $\hat{c}_{ij}^b = \frac{1}{N_T} \sum_{k=1}^{N_T} (n_i^k - \hat{m}_i)(n_j^k - \hat{m}_j)$  yields a biased estimator:

$$\begin{aligned} \langle \hat{c}_{ij}^b \rangle &= \frac{1}{N_T} \sum_{k=1}^{N_T} \langle (n_i^k - \hat{m}_i)(n_j^k - \hat{m}_j) \rangle = \frac{1}{N_T} \sum_{k=1}^{N_T} \langle n_i^k n_j^k \rangle - \langle \hat{m}_i \hat{m}_j \rangle = \frac{1}{N_T} \sum_{k=1}^{N_T} \langle n_i^k n_j^k \rangle - \frac{1}{N_T^2} \sum_{k,l=1}^{N_T} \langle n_i^k n_l^l \rangle \\ &= \frac{N_T - 1}{N_T} (\delta_{ij} \overline{a} + (1 - \delta_{ij}) \overline{c}) \end{aligned} \quad (32)$$

with  $\hat{m}_i = \frac{1}{N_T} \sum_{k=1}^{N_T} n_i^k$  and  $\langle n_i^k n_j^l \rangle = \delta_{ij} (\delta_{kl} \overline{a} + \overline{\delta m^2}) + (1 - \delta_{ij}) \delta_{kl} \overline{c} + \overline{m^2}$ . The unbiased estimator is therefore given by  $\hat{c}_{ij} = \frac{N_T}{N_T - 1} \hat{c}_{ij}^b = \frac{1}{N_T - 1} \sum_{k=1}^{N_T} (n_i^k - \hat{m}_i)(n_j^k - \hat{m}_j)$  [47]. Using this definition, along the same lines a lengthy, but straightforward analogous calculation shows that the variance of cross-covariances ( $i \neq j$ ) defined as  $\widehat{\delta c^2} = \frac{1}{N(N-1)} \sum_{i \neq j=1}^N (\hat{c}_{ij} - \hat{c})^2$  with the mean cross-covariance across neurons  $\hat{c} = \frac{1}{N(N-1)} \sum_{i \neq j=1}^N \hat{c}_{ij}$  yields the biased estimator

$$\langle \widehat{\delta c^2} \rangle = \left(1 - \frac{2}{N(N-1)}\right) \left(\overline{\delta c^2} + \frac{\overline{a^2} - \overline{c^2}}{N_T - 1}\right) \quad (33)$$

of the true variance of cross-covariances  $\overline{\delta c^2}$ . For a finite number of trials, there is a significant bias of  $\langle \widehat{\delta c^2} \rangle$  caused primarily by the average variance  $\overline{a}$  of spike-counts across trials (see Fig. S2a for an empirical estimate of the bias with trial-shuffled data).

The aim is hence to correct for the bias of the estimator. This can be formally done using Eq. (33), which we validate for synthetic data in Fig. S2b. A fit of Eq. (33) to the variance of cross-covariances obtained from subsampled numbers of trials of the experimental data shows that the true variance of cross-covariances can be approximately obtained by subtracting the mean of the distribution of the surrogate data in Fig. S2a.

In conclusion, the finite number of trials yields a significant bias to the variance of cross-covariances, but not to the mean autocovariances, if properly defined (see Eq. (32)). Fitting data to Eq. (33) and extrapolating for  $N_T \rightarrow \infty$  yields the unbiased estimate which we use in the main text. However, even neglecting this correction, the order of magnitude of the ratio between the two estimates, which determines the largest eigenvalue (Eq. (4) in the main text) and the operational regime, is not changed by the bias.

In addition to the bias in the estimation of the variance, the estimator comes with a statistical uncertainty due to the limited number of recorded neurons. We observe  $n = N(N-1)$  cross-covariances of which we want to estimate the true variance. The relative standard error of the variance is therefore given by  $\sqrt{2/(n-1)} \approx 0.009 < 1\%$  [48]. Error propagation to the estimation of  $R^2$  shows that the relative error of  $R^2$  is even smaller for  $R^2 > 1/3$ , and hence in the critical regime close to  $R^2 \simeq 1$  this error is negligible.

Qualitatively similar distributions of correlations have been obtained for other cortical areas, e.g. in visual cortex of macaque [26]. In this study, the authors consider correlations coefficients  $\hat{z}_{ij}$  rather than covariances  $\hat{c}_{ij}$ , and showed that mean correlations are close to zero. Furthermore, they showed a substantial contribution to the dispersion of correlation coefficients arising from finite data (see Fig. S3 in [26]). The remaining variance after this bias correction can be compared to our data if we re-interpret the spike counts  $n_i^k$  in the above calculations by the normalized spike counts  $n_i^k \rightarrow \frac{n_i^k}{\sqrt{\hat{c}_{ii}}}$ . Then the same derivation as above holds and we obtain an expression for the width of the biased estimator of the variance  $\overline{\delta z^2}$  of correlation coefficients in terms of the true variance  $\overline{\delta z^2}$  of correlation coefficients

$$\langle \overline{\delta z^2} \rangle = \left( 1 - \frac{2}{N(N-1)} \right) \left( \overline{\delta z^2} + \frac{1 - \bar{z}^2}{N_T - 1} \right). \quad (34)$$

For macaque motor cortex, we obtain a mean correlation coefficient  $\bar{z} = 0.007$  and a standard deviation  $\delta z_{ij} = \sqrt{\overline{\delta z^2}} = 0.10$ . Both values are on the same order of magnitude as in [26] ( $\bar{z} = 0.01$ ,  $\delta z_{ij} = 0.06$ ), but the dispersion is larger in motor cortex. This motivates more detailed future investigations of the distributions of correlations in various areas in relation to their effective network size.

### III. NUMERICAL SIMULATIONS

#### A. Figure 2

To illustrate the general mechanism relating network heterogeneity, eigenvalues, and distributions of covariances, we consider a simple network model with a sparsely and randomly connected inhibitory population of size  $N = 1000$  and covariance of single-unit fluctuations  $D = 1$ . Connections  $W_{ij}$  <sup>i.i.d.</sup>  $\mathcal{B}(p, w)$  are drawn independently from the same Bernoulli distribution with connection probability  $p = 0.1$  and weight  $w = -1/\sqrt{N}$  (first row),  $w = -2/\sqrt{N}$  (second row),  $w = -2.5/\sqrt{N}$  (third row) and  $w = -3/\sqrt{N}$  (fourth row).

#### B. Figure 3

All networks have sparse random connections of uniform strength drawn from Bernoulli distributions. Furthermore, neurons have a fixed number of incoming connections (in-degree) and do neither connect to themselves (no autapses) nor are they connected multiple times to other neurons (no multapses). The maximum eigenvalue on the abscissa (panels A-C) is varied by the choice of the connection strength.

*Homogeneous inhibitory network:* We consider inhibitory populations of size  $N = 1000$  (panels A,B) or  $N = 10000$  (panels C,E),  $D = 1$ , connection probability  $p = 0.1$  and uniform non-zero weights varied in the range  $w = -0.1, \dots, -0.001$  (panels A,B) or  $w = -0.03, \dots, -0.003$  (panel C). Panel E shows data for  $w = -0.0285$ .

*Excitatory-inhibitory network:* We consider a network of  $N_E = 8000$  excitatory and  $N_I = 2000$  inhibitory neurons with  $D = 1$ , connection probability  $p = 0.1$ , uniform excitatory connection strengths varied in the range  $w_E = 0.001, \dots, 0.01$  and uniform inhibitory connection strengths varied in the range  $w_I = -0.06, \dots, -0.006$ . Panel F shows data for  $w_E = 0.009$  and  $w_I = -0.05$ .

*Inhibitory network with distance-dependent connectivity:* We consider a network of  $N = 10000$  inhibitory neurons ( $D = 1$ ) randomly positioned on a  $1 \text{ mm} \times 1 \text{ mm}$  sheet. Each neuron receives  $K = 100$  incoming connections of uniform strength varied in the range  $w = -0.1, \dots, -0.01$ . Connections are drawn from a connection profile  $p(x) \sim \exp(-x^2/(2\sigma_{\text{conn}}^2))$  where  $x$  is the Euclidean distance between the presynaptic and postsynaptic neuron, and  $\sigma_{\text{conn}} = 50 \mu\text{m}$  the space constant.

*Leaky integrate-and-fire network:* We consider a network of  $N = 10000$  inhibitory leaky integrate-and-fire model neurons with delta-shaped postsynaptic currents. The membrane potential of each neuron follows the differential equation

$$\tau_m \frac{dV_i}{dt} = -V_i + \tau_m \sum_j J_{ij} s_j(t - h),$$

where  $s_j(t) = \sum_k \delta(t - t_k^j)$  is the spike train of the  $j$ -th neuron and  $t_k^j$  denotes the  $k$ -th spike of neuron  $j$ , which occurs whenever  $V_j$  exceeds the threshold  $\theta$ . The membrane potential is reset  $V_j(t_k^j +) \leftarrow V_r$  to the reset potential  $V_r$ .

Neuron model		
Name	Value	Description
$\tau_m$	20 ms	membrane time constant
$\tau_r$	2 ms	absolute refractory period
$V_r$	0 mV	reset potential
$\theta$	15 mV	fixed firing threshold
$E_{\text{leak}}$	0 mV	leak potential
Simulation parameters		
Name	Value	Description
$h$	0.1 ms	simulation time step
$T$	1000s	simulation time after initial transients
$T_{\text{trial}}$	1s	time window to compute spike counts

Table T1. Specification of neuron and simulation parameters for network of LIF model neurons shown in Fig. 3 of the main text.

after each such event and held at this level for the absolute refractory time  $\tau_r$ . The time lag  $h$  equals the resolution of the time-driven simulation. We choose a connection probability  $p = 0.1$  and uniform weights  $J \in [-1.1, -0.1]$ . Neuron and simulation parameters are shown in Table T1.

### C. Figure 4

Linear instability is determined by an eigenvalue close to the critical line  $\text{Re}(\lambda) = 1$ . For the dynamically balanced network close to the critical point (Fig. 4 left) we consider a sparse, random network of  $N = 1000$  inhibitory neurons with independent and identically distributed connections  $W_{ij} \stackrel{\text{i.i.d.}}{\sim} \mathcal{B}(p, w)$ . This network by definition has an inhibition-dominated feedback. The connection probability  $p = 0.1$  and weight  $w = -3.1/\sqrt{N}$  are chosen such that the theoretical prediction for the largest bulk eigenvalue is  $\lambda_{\text{max}} = \sqrt{Np(1-p)w^2} = 0.93 \lesssim 1$ . Due to the finite size of the network, the largest real eigenvalue, which is used in Fig. 4C, slightly differs from this result ( $\lambda \approx 0.917$ ).

For networks with almost vanishing feedback (Fig. 4 right), we consider a sparse, random network of  $N = 1000$  excitatory neurons with a feedback of order  $1 \ll N$ , where  $N$  is the network size. Connections  $W_{ij} \stackrel{\text{i.i.d.}}{\sim} \mathcal{B}(p, w)$  are independent and identically distributed. The connection probability  $p = 0.1$  and weight  $w = 9.17/N$  are chosen such that the feedback  $N\mu = Npw = 0.917 \lesssim 1$  almost compensates the neuronal leak (Eq. (6)). The critical eigenvalue in this network is given by the feedback  $N\mu$  and corresponds to the population activity.